Redistributed Pulsewidth Modulation of MMC Battery Energy Storage System Under Submodule Fault Condition

Feng Gao, *Senior Member, IEEE*, Xin Gu, Zhan Ma, *Student Member, IEEE*, and Chenghui Zhang, *Senior Member, IEEE*

***Abstract*—Battery energy storage system based on the modular multilevel converter (MMC-BESS) is able to realize the decentralized management of battery packs, which is suitable for the retired battery utilization to improve the efficiency of battery recycling. With multiple submodules (SM), the corresponding SM fault ride-through method is mandatory to improve operational reliability. This paper proposes a redistributed pulsewidth modulation method for MMC-BESS to ride-through the SM fault through employing the simple logic operation, which could avoid the unexpected carrier shift under various modulation indexes induced by the SM fault or grid voltage rise. MATLAB simulations and experimental results are presented to verify the performance of the proposed method.**

***Index Terms*—Battery energy storage system, fault ride-through, modular multilevel converter, pulse width modulation.**

I. Introduction

AIMING to solve the intermittent and fluctuating problems of the renewable energy utilization, battery energy storage system (BESS) can cooperate with the renewable power generation to restrain their power fluctuation and improve the stability of the power grid [1]. In addition, with the popularization and application of electric vehicles, numerous batteries are put into the market. In China, for example, the number of electric vehicles is from 12 800 in 2011 to 794 000 in 2017 and the power battery production is from 0.35 GWh in 2011 to 44.5 GWh in 2017. As a consequence, the retired batteries from electric vehicles can be appropriate to compose the energy storage station, thus achieving full use of resources and bringing effective economic benefits.

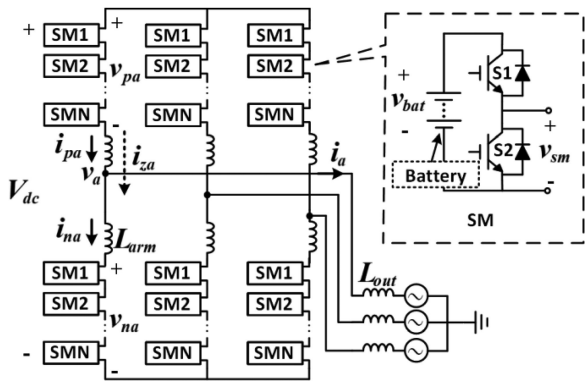

Fig. 1. Topological illustration of MMC-BESS.

Nevertheless, retired batteries from different manufacturers and circumstances have poor consistency, limiting the large-scale integrated application into the power grid. In this regard, focusing on the power conversion system is a feasible alternative [2]–[4]. Compared with two-level converter, modular multilevel converter (MMC) has more excellent output performance and flexible control capability. Trintis *et al.* [5] proposed to integrate MMC and BESS in 2011. As shown in Fig. 1, battery energy storage system based on the modular multilevel converter (MMC-BESS) disperses battery packs into submodules (SM) to facilitate the management of battery packs, helping to improve the total available capacity [6], [7]. Specifically, state-of-charge (SOC) balancing control for MMC-BESS was explored in [7] and [8], whereas the state-of-health (SOH) balancing methods inside and among the SMs were investigated in [9]–[11]. Some researchers proposed to implement the MMC-BESS topology into the battery electric vehicles to simplify the traditional battery manage system [12]–[15]. Also, MMC was introduced to integrate the battery and supercapacitor hybrid energy storage system, which can mitigate both the active and reactive power fluctuation [16], [17].

The SM of MMC-BESS can be built by either directly connecting batteries and half-bridge circuit [8]–[12] or inserting a bidirectional dc/dc converter between batteries and half-bridge circuit [18]–[20]. The former will make batteries suffer the low

Manuscript received November 14, 2018; revised April 1, 2019; accepted June 16, 2019. Date of publication June 25, 2019; date of current version December 13, 2019. This work was supported in part by the National Natural Science Foundation of China under Grant 51722704, in part by the Shandong Provincial Natural Science Foundation, China, under Grant JQ201717, in part by the Foundation for Innovative Research Groups of National Natural Science Foundation of China under Grant 61821004, and in part by The Key Project of National Natural Science Foundation of China under Grant 61733010. This paper was presented in part at the IEEE Energy Conversion Congress and Exposition, Cincinnati, OH, USA, Oct. 2017. Recommended for publication by Associate Editor D. Costinett. *(Corresponding author: Feng Gao.)*

F. Gao, X. Gu, and Z. Ma are with the Key Laboratory of Power System Intelligent Dispatch and Control, Ministry of Education, Shandong University, Jinan 250061, China (e-mail: fgao@sdu.edu.cn; xgu_sdu@foxmail.com; mazhan_ee@163.com).

C. Zhang is with the School of Control Science and Engineering, Shandong University, Jinan 250061, China (e-mail: zchui@sdu.edu.cn).

Color versions of one or more of the figures in this paper are available online at http://ieeexplore.ieee.org.

Digital Object Identifier 10.1109/TPEL.2019.2925284

frequency power oscillation and the latter will increase the control complexity and construction cost. Regardless of the specific SM configuration, the MMC-BESS should have the SM fault ride-through capability for its reliable operation.

Control methods of traditional MMC under SM fault condition have been studied a lot [21]–[27], and the common way to prevent the operational failure is to increase the redundant SM number. The concepts of cold reserve and spinning reserve of MMC were proposed in [21]. Cold reserve means the redundant SM is bypassed under normal operation and when an SM fails, and the faulty SM is replaced by the redundant SM [22], [23], which has disadvantages of transient effect and long charging time. An improved method for cold reserve was proposed in [23] to decrease the transition effect by changing the reference of normal SMs on the faulty arm but the switching harmonics was still produced in the transient process and the high modulation depth operation was not discussed. Spinning or hot reserve means the redundant SM is also involved into operation under normal operation conditions, and after the faulty SM is bypassed, the dc voltage is shared by the remaining SMs [23], [24]. In specific, one scheme of hot reserve only bypasses the faulty SM and keeps other arms unchanged, which will make MMC asymmetrical. An energy balancing method to overcome the asymmetry was proposed in [21] and the rotating sliding choice box was proposed in [24] to distribute the state and carrier of each SM to ride-through the fault, whereas another scheme of hot reserve will maintain its normal working status by bypassing the same number of SMs per arm.

In principle, the traditional fault-tolerant methods of MMC are based on the redundant or reserved SMs, which indeed can also be implemented in MMC-BESS. But being different, this paper proposes the redistributed pulsewidth modulation (R-PWM) method to take advantage of the MMC-BESS characteristics, such as the very slow battery voltage variation and no integrated dc source in common dc link to compensate the output performance degradation which may occur during SM fault. In specific, the proposed method could provide the following benefits during operation.

1) The proposed redistributed PWM method can simply realize the ride-through operation by employing simple logic operation unlike other methods that should either readjust the PWM carriers or change the DSP algorithms.
2) The proposed method employs all SMs during the normal operation, which could smoothly overcome the influence induced by both SM fault and grid voltage variation, especially when suffering the grid voltage rise, whereas other methods have to shift their carriers' angle to fully use the redundant SM and then will unavoidably introduce the unexpected transient distortion.

This paper first introduces the traditional control methods of MMC-BESS for both the normal operation and fault ride-through operation, and then the redistributed PWM method is elaborated by considering the different modulation index. Finally, MATLAB/Simulink simulations and experimental results are presented to verify the performance of the proposed method.

II. Basic Control Method of MMC-BESS

In Fig. 1, the upper and lower arm voltages can be expressed as

$$v_{pa} = \frac{1}{2}V_{\rm dc} - v_a - L_{\rm arm}\frac{di_{pa}(t)}{dt} \tag{1}$$

$$v_{na} = \frac{1}{2}V_{\rm dc} + v_a - L_{\rm arm}\frac{di_{na}(t)}{dt} \tag{2}$$

where v_{pa}, i_{pa}, v_{na}, and i_{na} are the voltage and current of the upper or lower arm of phase A, $V_{\rm dc}$ is the dc voltage of MMC-BESS, and v_a is the ac output voltage of phase A, which can be expressed as

$$v_a = V_m \sin \omega t \tag{3}$$

where V_m is the amplitude of ac output phase voltage. Unlike the traditional MMC, MMC-BESS has no integrated dc source, and the dc voltage of MMC-BESS is composed of the battery voltages of SMs. According to (1) and (2), neglecting the voltage drop across the arm inductor, it can be concluded that the upper and lower arm voltages are the same dc voltage plus the opposite sinusoidal ac voltage, as expressed in the following equations:

$$v_{pa} = \frac{1}{2}V_{\rm dc} - v_a \tag{4}$$

$$v_{na} = \frac{1}{2}V_{\rm dc} + v_a \tag{5}$$

Similarly, the equations for v_{pb}, v_{nb} and v_{pc}, v_{nc} can also be easily derived, and it is obvious that the line voltage is the difference of the two arm voltages in the same direction, such as v_{ab} in (6). The dc voltage is the sum of the upper and lower arm voltages in the same phase in (7)

$$v_{ab} = v_{na} - v_{nb} = v_{pb} - v_{pa} \tag{6}$$

$$V_{\rm dc} = v_{pa} + v_{na} = v_{pb} + v_{nb}. \tag{7}$$

Besides, output voltage of each SM has two states of 0 and $v_{\rm bat}$; hence, the range of arm voltage v_{pa} and v_{na} in (1) and (2) vary between 0 and $Nv_{\rm bat}$ when the SM battery packs are balanced. Observing (1)–(3), since the range of arm voltages is limited, the value of dc voltage can influence the range of ac output voltage. In general, dc voltage is set as

$$V_{\rm dc} = Nv_{\rm bat}. \tag{8}$$

In this case, dc part of the arm voltage is located at the midpoint of the output voltage range so that the ac output voltage amplitude can be maximized. Therefore, in the MMC-BESS, the dc voltage is generally performed according to (8). However, this constraint is not mandatory, and dc voltage can be changed under special circumstances.

A. Modulation Method

Fig. 2 introduces the modulation and control process of MMC-BESS. First, the controller is set to track a control target, such as output voltage, output current or open-loop target, and the reference signal is calculated accordingly. Then the modulator receives the reference to generate the digital switching signal,

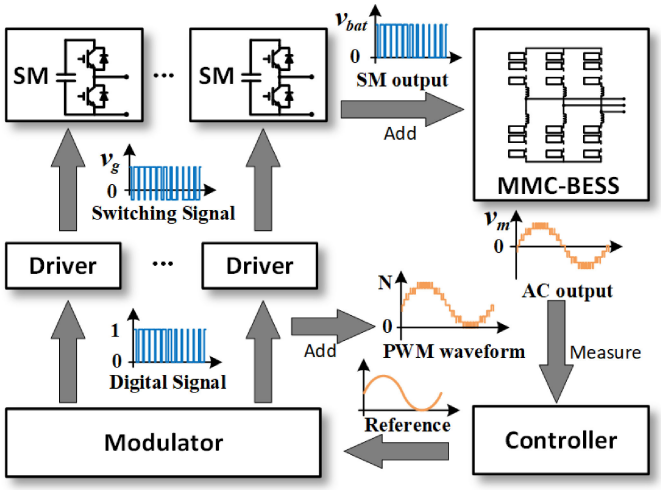

Fig. 2. Modulation and control process of MMC-BESS.

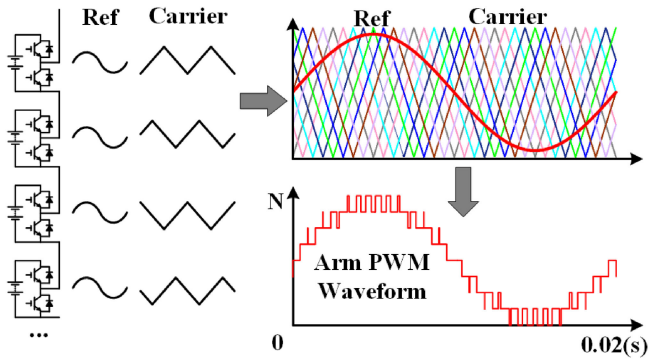

Fig. 3. Illustration of carrier phaseshift PWM.

thus driving the switching devices of SM through the gate driver, and the corresponding ac output of MMC-BESS is produced by the sum of all SM outputs.

The role of the modulator is to amplify the digital signal to an analog voltage output, thus to make the ac output approaching the reference wave [28]. In MMC-BESS, at the moment when the modulator's digital signal is a high level of 1, the SM output is the battery pack voltage $v_{\rm bat}$, as shown in Fig. 2. Therefore, the digital signals calculated by the modulator are essential as they can directly affect the output waveform quality of MMC-BESS.

Leon *et al.* [29] comprehensively reviewed the modulation technologies for voltage-source inverters. As for the modulation methods of MMC-BESS, carrier phaseshift pulsewidth modulation (CPS-PWM) [30]–[32] or nearest level modulation are usually used. Fig. 3 shows the principle of CPS-PWM per arm. The output waveform of each SM is obtained by using different carrier waves comparing with the same reference wave. CPS-PWM has two schemes of $N+1$ and $2N+1$ modulation, which are different in terms of the carrier phase displacement between the upper arm and lower arm. The $2N+1$ method has better output waveform but brings larger circulating current, whereas the $N+1$ method is on the contrary.

It is noted from Fig. 3 that the essence of CPS-PWM is to make the arm output waveform composed of the adjacent two levels thus to decrease harmonics remarkably by adding the shifted waveform of each SM and then increase the equivalent switching frequency. The difference between CPS-PWM and the nearest level modulation is that the former makes output impulse equally with the reference all the time whereas the latter does not; therefore, CPS-PWM is more suitable for MMC-BESS since the SM output waveforms are highly consistent, which are convenient for battery management.

When taking phase A as an example, by using the CPS-PWM, the arm voltage can be calculated as

$$v_{pa} = \sum_{i=1}^{N} v_{\rm bat\_pi} \frac{1 - m\sin\omega t}{2} \tag{9}$$

$$v_{na} = \sum_{i=1}^{N} v_{\rm bat\_ni} \frac{1 + m\sin\omega t}{2} \tag{10}$$

where m is the modulation index, which represents the ratio of the reference amplitude to the carrier amplitude. Assuming that all SM voltages are balanced and the voltage on arm inductor is neglected, the phase voltage can be expressed as

$$v_a = \frac{1}{2} N v_{\rm bat} m \sin(\omega t + \varphi). \tag{11}$$

From (3) and (11), the modulation index can also be expressed as

$$m = \frac{2V_m}{N v_{\rm bat}}. \tag{12}$$

Hence in MMC-BESS, in order to achieve the same ac output, the more SMs that participate in the operation, the lower the modulation index. If all SMs are put into operation, the modulation index represents the redundancy in MMC-BESS configuration.

B. SM Fault Ride-Through Methods

In the traditional MMC, redundant SMs are configured to ride-through the SM failure, which can be also used in MMC-BESS. The number of redundant SMs in MMC-BESS can be calculated as follows. First, the modulation index should be less than 1, otherwise there will be overmodulation and increase output harmonics substantially. In addition, SM battery pack voltage will change with the variation of its SOC. Assuming that the battery pack voltage is $v_{\rm bat\_min}$ when discharging to the lowest SOC, then according to (12), the SM number in each arm of MMC-BESS should meet

$$N \geq \frac{2v_m}{v_{\rm bat\_min}}. \tag{13}$$

The minimum positive integer N_0, which satisfies the condition of (13) is the SM number per arm without redundancy in MMC-BESS. If the actual SM number per arm is N, the redundant SM number will be $(N - N_0)$.

Learning from the traditional MMC, the ride-through strategies of MMC-BESS when suffering the SM fault can be divided as follows.

1) Cold Reserve: If the cold reserve method is used, a bypass switch is required for each SM. The bypass switch needs to be

disconnected when the SM is normal and bidirectionally conducted when the SM fails. Therefore, two high-current switching devices are often required, and the whole cost is greatly increased. Besides, the state of the new input SM battery pack may be significantly different from the other SMs, which have already been put into operation for a long term, affecting the output quality and bringing transient influence.

2) Hot Reserve With the Number of SMs Participated Into Operation Being N_0: A common method is to use the half-bridge circuit to achieve the role of the bypass switch. This method can reduce the cost of the bypass switch compared to cold reserve but still has the inconsistent state of input SM. Besides, the sliding selection box [24] can also be adopted in MMC-BESS to select the operating SMs and the corresponding phase-shift angles of carriers for normal or faulty states. Through the sliding selection box, different N_0 SMs are selected to output in each cycle, and when the SM fails, the faulty SM will be removed from the candidate queue. By using this method, each normal SM (whether it is a redundant SM or not) will participate in the operation, and the problem of the inconsistent state of the redundant battery pack can be solved. But when suffering the grid voltage rise, the sliding selection box method has to put all SMs into operation and adjust the carriers' angles to fit the high modulation index, which will unavoidably induce the output distortion during the transient process.

3) Hot Reserve With the Number of SMs Participated Into Operation Being N: As described above, under the same output voltage, the greater the number of SMs participating in the output, the smaller the modulation index. Therefore, during normal operation, the redundant SMs can all be put into operation and the real-time modulation index can be calculated through closed-loop feedback. Under this redundant strategy, when an SM is failed and bypassed, one method is to bypass the same number of SMs in other five arms and another is to leave the other arms unchanged. The former can ensure the symmetry of the system but six times of failed SMs no longer participate in the operation. In addition, the carrier phaseshift angles of all SMs after the removal will also change, and the control will be more complex and the unexpected transient effect will occur. The latter will lead to the asymmetrical operation of MMC-BESS, which will decrease the waveform quality, generate harmonics and circulating current, and affect the battery lifetime.

To sum up, for the SM fault ride-through strategy of MMC-BESS, the following principles should be followed.

1) Use hot reserve to avoid the cost of the bypass switch.
2) The redundant SM number should be reduced as much as possible.
3) If the system is configured with redundant SMs, it is a better choice for all redundant SMs to participate in the output operation. Furthermore, after bypassing the fault SM, the system symmetry and output waveform quality should be maintained. And the transient distortion induced by the carriers' angle shifts when suffering modulation index variation should be attenuated as well.

Based on the above principles, the R-PWM method is proposed. The R-PWM method utilizes the characteristics of MMC-BESS, such as the slow battery voltage variation and no integrated dc source in common dc link. Besides, SMs in the operating mode rather than the standby mode are used to decrease the influence of the bypassed faulty SMs. The detailed operational principles will be elaborated in Section III.

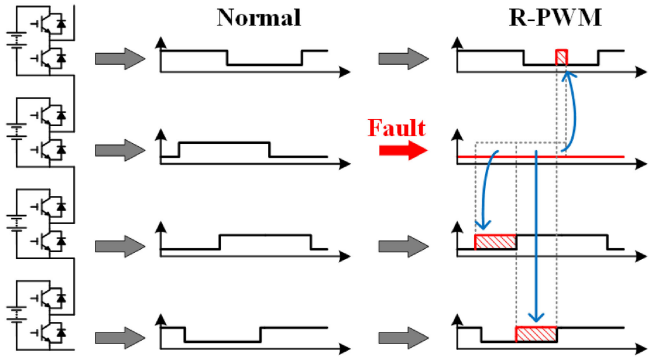

Fig. 4. Basic working principle of R-PWM method.

III. Redistributed Pulsewidth Modulation

MMC-BESS is different from the traditional MMC by replacing the dc capacitors to batteries and the SM battery voltage will not change rapidly within a short-time interval after the fault, thus modifying the modulation method can be effective to ride-through the SM fault without worsening the circulating current. When an SM fails, the expected high-level output of the faulty SM becomes 0 by bypassing the SM, hence the corresponding arm voltage is reduced by $v_{\rm bat}$ and the ac output voltage will be deteriorated. To improve the output quality, the original high-level output of faulty SM can be reassigned to other normal SMs, as shown in Fig. 4. This is the basic principle of R-PWM.

The control block diagram of MMC-BESS when assuming the R-PWM method and the corresponding logic operation process are shown in Fig. 5(a) and (b), respectively. Compared with the original modulation method, two processes with several logical gates are added to produce the R-PWM output of each SM. Process 1 is the basic R-PWM method, and Process 2 is the compensation method, where Fault Signal will be set to 1 when an SM in the arm fails, k is the serial number of faulty SM, and the compensation signals *Comp_in* and *Comp_out* will be described later. These two logic operation processes will be elaborated below.

A. Basic R-PWM Method

Basic R-PWM method is to assign the high-level output of faulty SM to the remaining normal SMs in the same arm. In Fig. 5(b), when the fault signal is set to 1 and k is confirmed, the output waveform of healthy SM_n can be changed accordingly and obtained during the following two steps.

1) Make the original output waveform of SM_{n-1} (when $n = 1$, $n-1$ turns to N) logically AND with the original output waveform of the fault SM_k.
2) Make the normal output waveform of SM_n logically OR with the output of the above step.

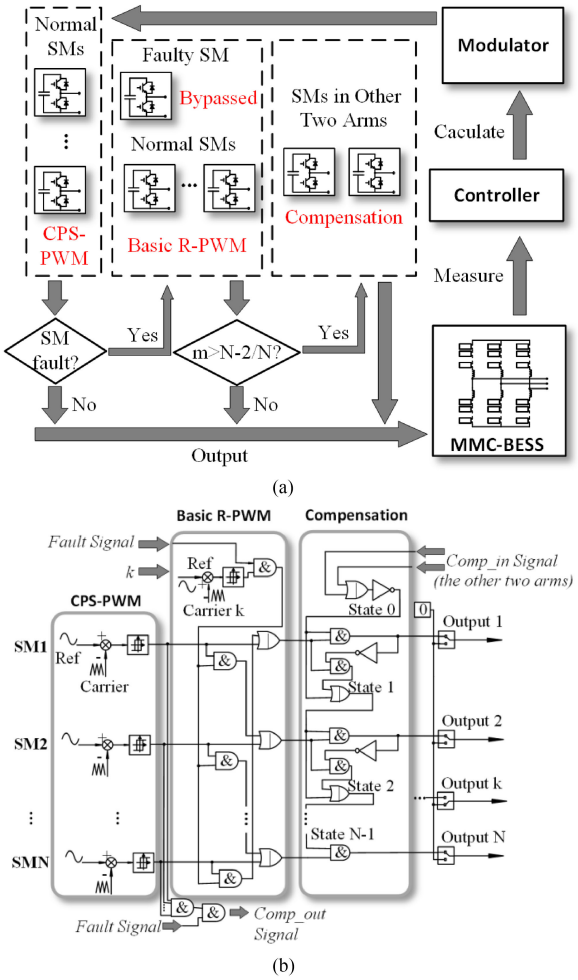

Fig. 5. (a) Control block diagram when assuming the R-PWM method. (b) Logical process of the R-PWM arm control.

All the remaining normal SMs in the faulty arm can use these two steps to get their R-PWM switching commands. The constraint of basic R-PWM is that the remaining normal SMs should have enough low-level output to compensate, hence the duty cycle can influence the performance. The analyses under different duty cycles are expressed as follows.

1) Duty Cycle Less Than (N – 1)/N: In one switching period, the reference signal and the duty cycle can be seen as constant. When the duty cycle is less than $(N-1)/N$, the normal output waveform of each SM and the corresponding arm output in one switching period are drawn in the left side of Fig. 6 ($N = 8$). When the SM4 fails and its PWM output turns to 0, the output waveform by using the basic R-PWM is shown on the right side of Fig. 6. The shaded switching intervals 1 to 5 are added in the healthy SMs and compensate the switching interval of the faulty SM4 by the two steps mentioned above. For example, the shaded switching interval 5 of SM1 is obtained by running AND operation between the switching commands of SM8 and SM4 and then running OR operation with the switching command of SM1. As a consequence, the arm output waveform after R-PWM is exactly the same as the normal operation condition as shown in Fig. 6.

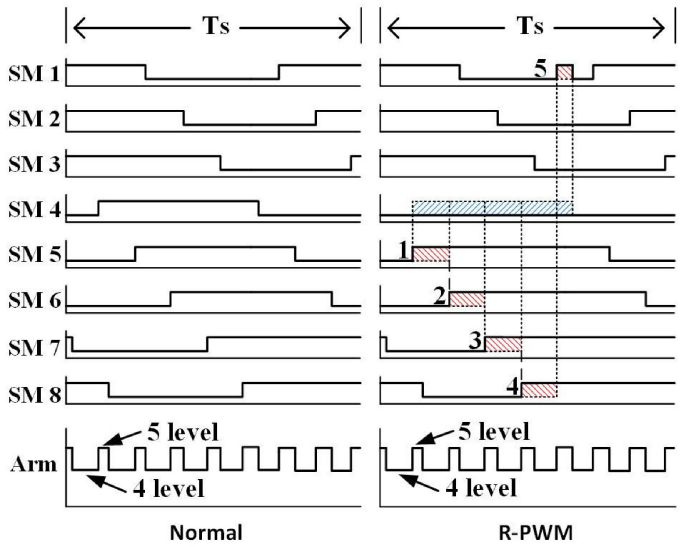

Fig. 6. Output waveform of each SM and corresponding arm output during one switching period when the duty cycle less than $(N-1)/N$.

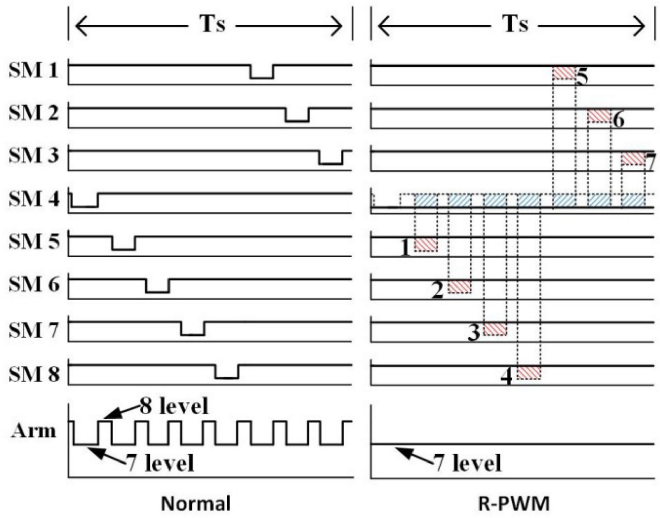

Fig. 7. Output waveform of each SM and corresponding arm output during one switching period when the duty cycle larger than $(N-1)/N$.

2) Duty Cycle Larger Than (N – 1)/N: Under this circumstance, the normal switching waveform and basic R-PWM waveform after SM fault during one switching period are comparatively shown in Fig. 7, where $N = 8$. It can be observed that the healthy SMs do not have enough zero switching intervals to compensate the waveform of faulty SM so that the normal arm output is composed of seven and eight levels but the R-PWM output only produces maximum seven levels. It is evident because the normal SMs remaining in the arm is not enough to reach the required level number.

Taking longer time into consideration, the modulation index will affect the range of the duty cycle. The relationship between the duty cycle and modulation index is

$$D = \frac{1}{2}(1 + m\sin\omega t). \tag{14}$$

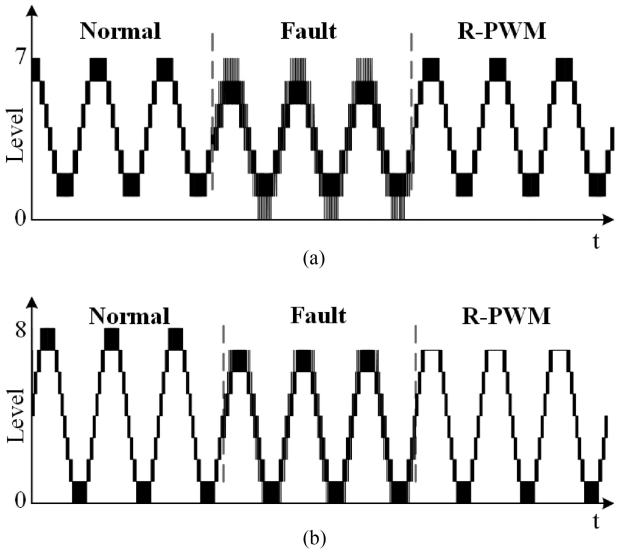

Fig. 8. Arm output PWM waveform during normal, faulty, and R-PWM states when (a) $m < (N-2)/N$ and (b) $m > (N-2)/N$.

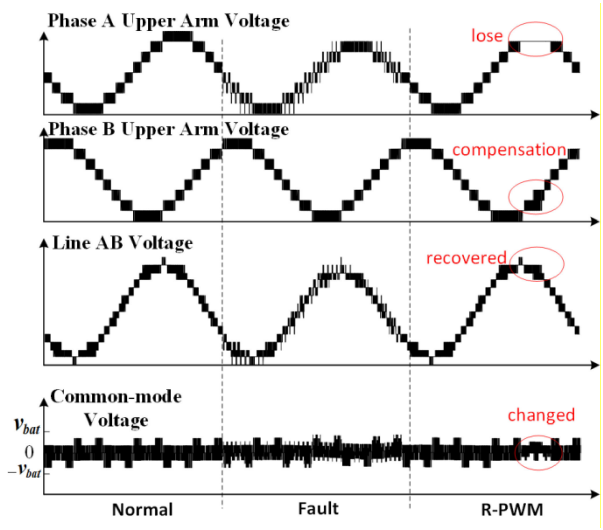

Fig. 9. Arm voltages, line voltage, and common mode voltage during normal, fault, and R-PWM operation conditions.

Since the range of sinusoidal functions is –1 to 1, the duty cycle can always be less than $(N-1)/N$ when the modulation index is less than $(N-2)/N$. As mentioned before, the modulation index represents the redundant configuration of MMC-BESS, so the basic R-PWM has different performances depending on the modulation index.

Fig. 8(a) draws the output PWM waveform of the faulty arm when the modulation index is less than $(N-2)/N$ in several fundamental periods. In specific, MMC-BESS works in the normal state, and then an SM fails and is bypassed; it can be observed that the output PWM waveform is deteriorated. After using the basic R-PWM operation, the output waveform is completely recovered to the normal state without any distortion.

On the other hand, Fig. 8(b) shows the corresponding output waveform when the modulation index is larger than $(N-2)/N$. Most levels of the output waveform by the basic R-PWM are the same as the normal state but the highest level cannot be reached, which will affect the output quality and bring dc circulating current among phases and fundamental circulating current among arms. Therefore, an additional compensation method is proposed in Section III-B.

B. Compensation Method When $m>(N-2)/N$

As mentioned above, by using the basic R-PWM method, 0 to $N-1$ level of arm output can be recovered. However, if the modulation index is larger than $(N-2)/N$, N level occurs in the arm output cannot be reached. When the normal arm output level is N, and the output level by the basic R-PWM is $N-1$, which can be considered that 1 level is reduced in the faulty arm. Therefore, if corresponding upper or lower arms of other two phases both reduce 1 level at the same time to compensate the highest level interval of the faulty phase, the line output is still identical with the normal state according to (6), which indeed is the operational principle for compensating the voltage level by using other phases. As the MMC-BESS is a three-phase three-wire system, the quality of three-phase currents will remain unchanged if the line voltages keep unchanged [33].

Therefore, the logic operation target is to find the SM, which should have high-level output and reduce it to a low level in the healthy phases during the highest-level interval of the faulty phase. In Fig. 5(b), *Comp_out* and *Comp_in* are the compensation signals of the arm itself and other two arms in the same direction. The compensation signal is set to 1 when the arm is faulty and all SMs' outputs are high level, which means it should be compensated by other two arms. Furthermore, State 0 to State $N-1$ in Fig. 5(b) are the compensation states per SM where 0 indicates that there is still one level needed to be reduced. The compensation method can be achieved with the following steps as shown in Fig. 5(b).

1) When the compensation signal of other two arms is not 0, set State 0 with 0, otherwise State 0 is 1.
2) Make the normal output of SM_1 run AND with the State 0 and produce the new output of SM_1.
3) Make the normal output of SM_1 run AND with the inversion of the new output, then run OR with State 0 to obtain the State 1.
4) Circulate steps 2 and 3 to obtain the output and state of each SM.

Through the above steps, two normal arms (either upper or lower arms) will find the first SM with high-level output and reduce it to a low level if necessary. If compensation is not needed, the state in Fig. 5(b) will be all 1 and the output will not change. Fig. 9 shows arm voltages, line voltage, and common mode voltage during normal, fault, and R-PWM states when the modulation index is higher than $(N-2)/N$. It can be seen that after the failure of the A-phase SM, the waveform is restored to the normal state by the basic R-PWM except for the highest level, and the portion not completely recovered is compensated by Phase B so that the line voltage is restored to the normal state. Also, it is observed that the common mode voltage will not change significantly.

TABLE I
SIMULATION PARAMETERS

Item	Value
Battery voltage per SM	100 V
Number of SMs per arm	8
Inductance per arm	8 mH
Switching frequency	2 kHz
Fundamental frequency	50 Hz
Fault time	0.02 s
R-PWM time	0.04 s

Using this method, the dc voltage will lose a voltage level during the compensation interval according to (7), which is not acceptable for the traditional MMC with an integrated dc source. But the proposed compensation method can be effective because MMC-BESS does not have the integrated dc source. Just like mentioned before, the dc-link voltage of MMC-BESS does not need to be constant. On implementation, the compensation method can be effective when the modulation index is less than $(N-1)/N$, which means as long as the MMC-BESS has one redundant SM per arm; the proposed method can work well without changing the PWM carriers' angle.

IV. SIMULATION VERIFICATION

Simulations are conducted by MATLAB/Simulink to verify the performance of R-PWM method. A three-phase MMC-BESS is constructed as shown in Fig. 1 and controlled by using the closed-loop control methods presented in Figs. 2 and 5, and the corresponding simulation parameters are listed in Table I. To avoid the influence of circulating current, an effective circulating current suppression method is adopted. To clearly show the performance of the proposed method, one SM in the upper arm of phase A fails at 0.02 s, and the R-PWM is triggered to work at 0.04 s.

A. $m \leq (N-2)/N$

First, by setting the amplitude of grid phase voltage to be 300 V, $m \leq (N-2)/N$. Fig. 10 shows the phase current, faulty arm voltage, and grid voltage of phase A and circulating current under different operation conditions. It can be observed that the circulating current is attenuated to nearly zero under the normal state. When one SM fails, the phase current is conducted with harmonics and circulating current increases significantly. By adopting the R-PWM at 0.04 s, arm voltage, phase current, and circulating current recover to their normal status.

The FFT analysis of phase A current is shown in Fig. 11, where the current has more harmonics in low frequency range under the fault condition and the output current after R-PWM operation is the same as the normal output current.

B. $m > (N-2)/N$

Alternatively, by setting the amplitude of grid phase voltage to be 350 V, the modulation index just equals to $(N-1)/N$ of 0.875.

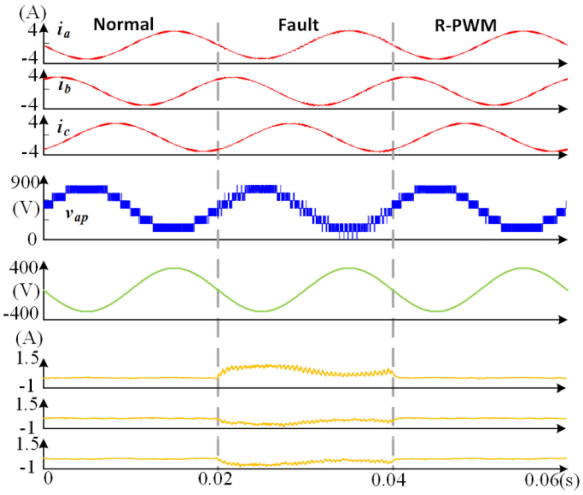

Fig. 10. Three-phase output currents, faulty arm voltage, grid voltage of phase A and three-phase circulating currents (from top to bottom) under normal, fault, and R-PWM conditions.

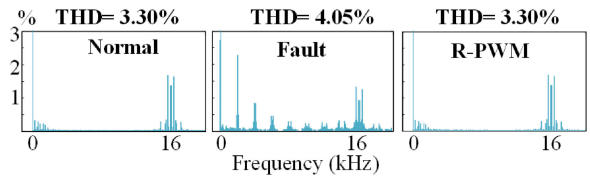

Fig. 11. FFT analysis of phase A current when $m \leq (N-2)/N$.

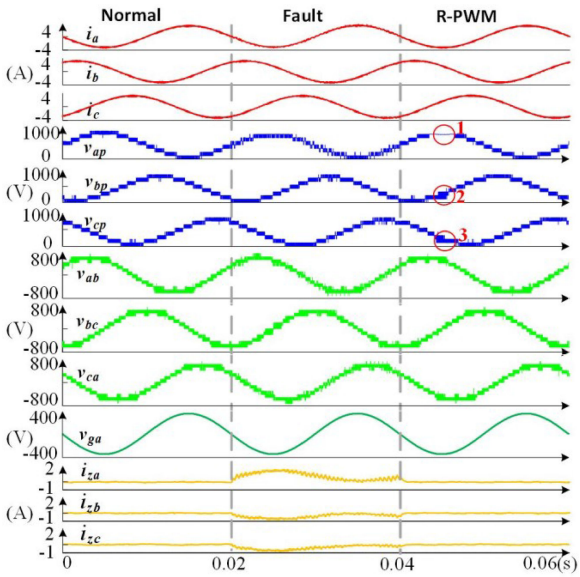

Fig. 12. Three-phase output currents, arm voltages, line voltages, grid voltage of phase A, and three-phase circulating currents (from top to bottom) under normal, fault, and R-PWM conditions.

Fig. 12 shows three-phase currents, arm voltages, three phase line voltages, grid voltage of phase A, and circulating currents under different conditions. It can be seen that by triggering the R-PWM method at 0.04 s, the output of the upper arm of phase A cannot operate as normal. Meanwhile, the arm voltage level

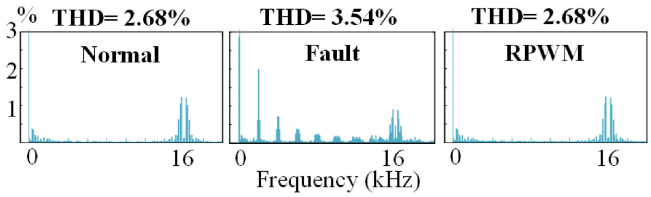

Fig. 13. FFT analysis of phase A current when $m > (N-2)/N$.

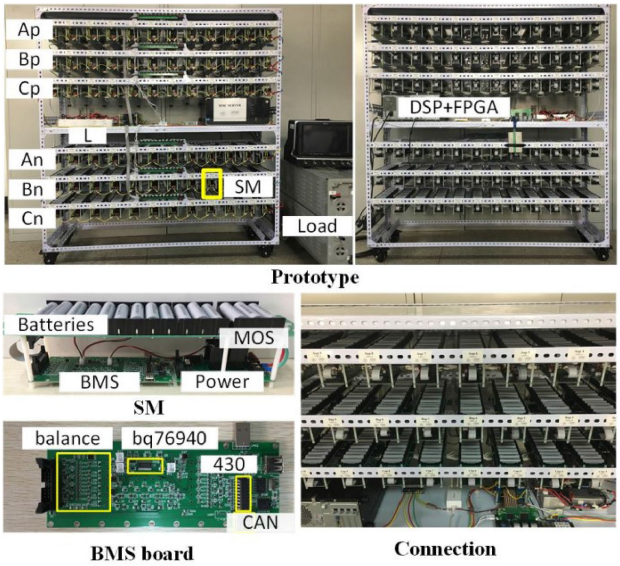

Fig. 14. Photograph of MMC-BESS prototype.

TABLE II
EXPERIMENTAL PARAMETERS

Item	Value
SM number per arm	12
Battery voltage per SM	55.5 V
Total energy	9.99 kWh
Grid voltage	380 V
Arm inductance	2 mH
Output inductance	1.3 mH
Switching frequency	5 kHz
Load	36 Ω

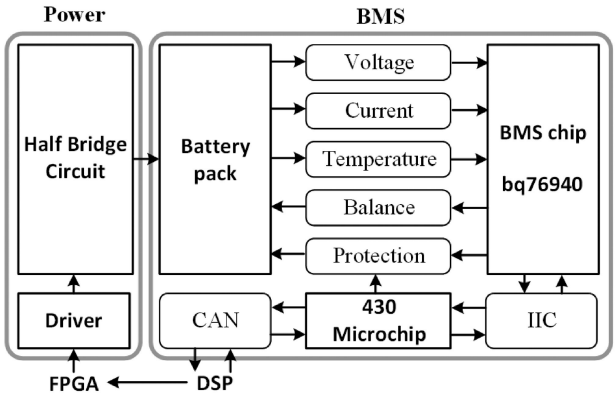

Fig. 15. SM control of MMC-BESS prototype.

of phases B and C are reduced in the highlighted areas 1 and 2 to compensate Phase A output. Therefore, by the R-PWM, the phase circulating current is attenuated to zero as expected and the line voltage is exactly the same as the normal state. The FFT analysis of phase A current is shown in Fig. 13 and the quality of output current after R-PWM is also recovered to its normal state.

V. EXPERIMENT VERIFICATION

A three-phase MMC-BESS prototype with 72 SMs was built to verify the performance of R-PWM method and Fig. 14 displays the photographs of the prototype, where the front and back sides of the prototype, SM, battery management system (BMS) board and SM connection details are shown, respectively.

Table II lists the experimental prototype parameters, in which each bridge arm contains 12 SMs and each pack in SM is composed of fifteen 18 650 Li-ion battery cells whose nominal voltage is 3.7 V. So, the nominal voltage per pack is 55.5 V and the prototype can be directly connected to 380 V (line–line rms voltage) grid without the transformer. When $2N+1$ modulation is adopted, the number of arm levels can reach 25.

In detail, Fig. 15 shows the SM control block of MMC-BESS prototype, whose two major functions are battery management and power control. In the BMS board, bq76940 is used to monitor the state of batteries and balance the SOC within the SM. Besides, each SM has a 430 microchip to read the measured data by the inter-integrated circuit communication with the BMS chip and send it to the host controller by controller area network communication. In the power board, MOSFET is selected as the switching device for its low cost and switching losses.

The control system of the prototype is composed of DSP and FPGA. The TMS320F28335 DSP is used as the host controller, which carries out to read and log the information of each SM's batteries, obtains the analog-to-digital results, calculates the reference of each SM and locates the SM fault. An XC3S500E-4PQG208C FPGA is adopted to produce the driven signal of each SM. In particular, the R-PWM is easily achieved in the FPGA by adding several logical gate operations.

Through designing FPGA program according to Fig. 5(b), corresponding experimental results were obtained by setting different conditions. In order to see the performance of R-PWM method clearly, the arm voltage and line voltage measured by the oscilloscope are the voltages before the arm inductors.

Setting the modulation index $m = 0.74$ ($m < (N-2)/N$, $N = 12$) refers to the amplitude of phase voltage being 245 V achieved by regulating the ac source. The upper arm voltage of phase A and phase B, line–line voltage, and faulty SM voltage during normal, fault, and R-PWM states are shown in Fig. 16 when SM_1 in the upper arm of phase A fails. It can be seen that during the faulty state, the output voltage of faulty SM is set to zero and the upper arm voltage of phase A has the unwanted switching waveform. In the R-PWM state, the faulty SM voltage is still zero but the arm voltage is completely recovered. Also, the circulating

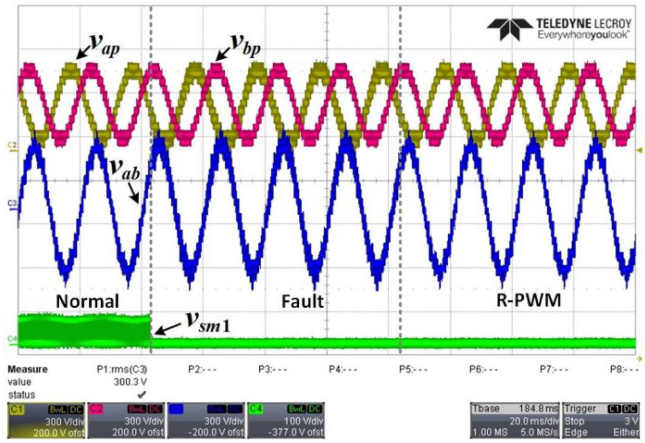

Fig. 16. Upper arm voltage of phase A (v_{ap}, 300 V/div) and phase B (v_{bp}, 300 V/div), line–line voltage (v_{ab}, 300 V/div), and faulty SM voltage (v_{sm1}, 100 V/div) during normal, fault, and R-PWM states when $m = 0.74$ (timescale: 20 ms/div).

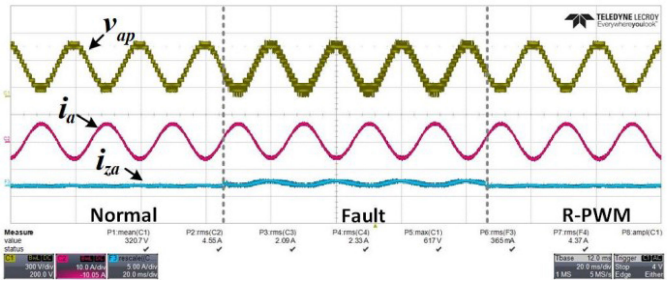

Fig. 17. Upper arm voltage (v_{ap}, 300 V/div), output current (i_a, 10 A/div), and circulating current (i_{za}, 5 A/div) of phase A during normal, fault, and R-PWM states when $m = 0.74$ (timescale: 20 ms/div).

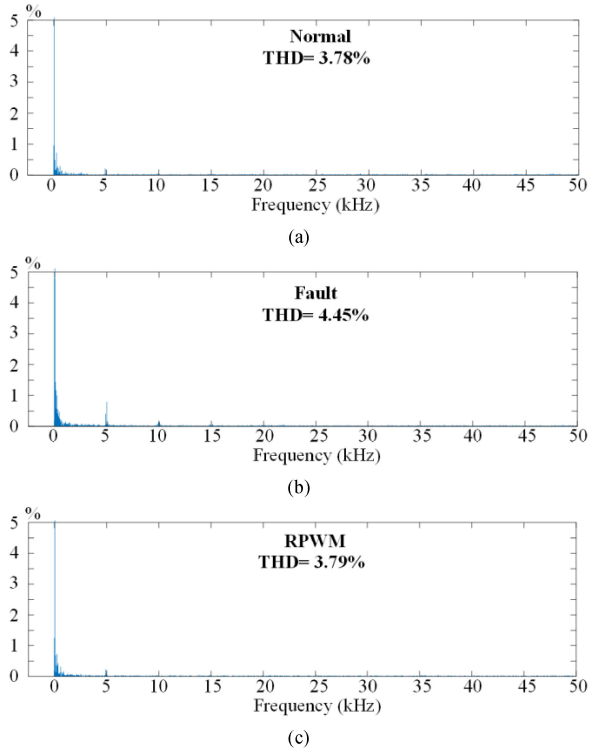

Fig. 18. FFT analysis of phase A current under normal, fault, and R-PWM conditions when $m = 0.74$.

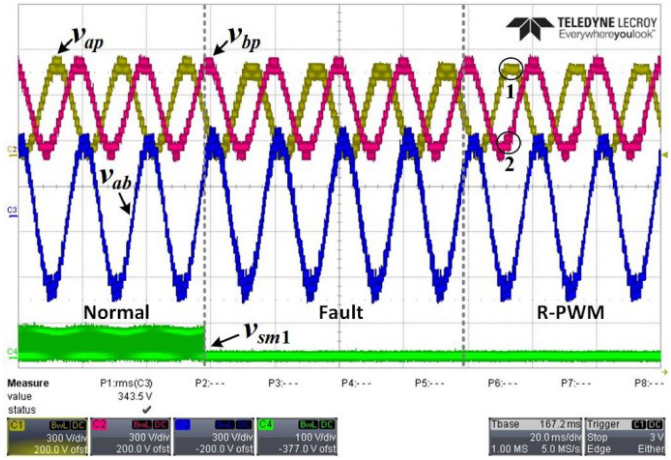

Fig. 19. Upper arm voltage of phase A (v_{ap}, 300 V/div) and phase B (v_{bp}, 300 V/div), AB line voltage (v_{ab}, 300 V/div), and faulty SM voltage (v_{sm1}, 100 V/div) during normal, fault, and R-PWM states when $m = 0.85$ (timescale: 20 ms/div).

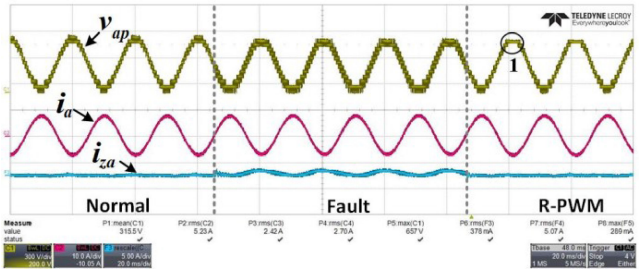

Fig. 20. Upper arm voltage (v_{ap}, 300 V/div), output current (i_a, 10 A/div), and circulating current (i_{za}, 5 A/div) of phase A during normal, fault, and R-PWM states when $m = 0.85$ (timescale: 20 ms/div).

current and output current of phase A are shown in Fig. 17. It is observed that the circulating current is increased significantly under the fault condition but can be attenuated to the normal condition when the R-PWM method is used. Furthermore, the FFT analysis of phase A current is shown in Fig. 18, where the current has more harmonics in low frequency range under the fault condition and the output current THD after R-PWM operation is as good as the normal output current.

Comparatively, the experimental results under the high modulation index of 0.85 ($(N - 1)/N > m > (N - 2)/N$, $N = 12$) are shown in Figs. 19 and 20, respectively, when the amplitude of phase voltage is 285 V. It can be observed from Fig. 19 that the arm voltage of phase B is changed in the highlighted area 2 in order to compensate the output waveform of phase A in the highlighted area 1. Such phenomenon is consistent with the performance of simulation results. In addition, the line voltage is recovered to the normal state as expected by using the R-PWM method after an SM fault. Also, it is noted that the circulating current after the R-PWM method can be attenuated significantly. Finally, the FFT analysis of phase A current in Fig. 21 shows that the quality of output current after R-PWM can be recovered to its normal state.

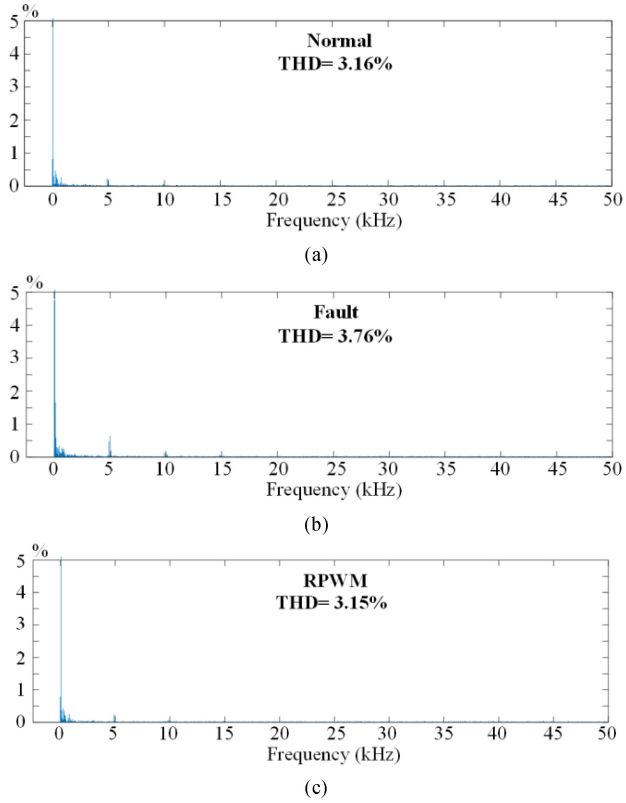

Fig. 21. FFT analysis of phase A current under normal, fault, and R-PWM conditions when $m = 0.85$.

VI. Conclusion

This paper proposes the redistributed PWM method for MMC-BESS under SM fault condition. In the MMC-BESS with the low modulation index, the basic R-PWM can recover the system to normal and symmetrical operation state without the involvement of other arms. Furthermore, under the high modulation index condition, a compensation method is added after the basic R-PWM logic operation to completely recover the system from SM fault. Therefore, the proposed R-PWM method can ride-through the SM fault by just employing the simple logic operation without adjusting the carriers' angles. MATLAB simulations and experimental results are presented to verify the performance of the proposed method.

References

[1] D. Tran and A. M. Khambadkone, "Energy management for lifetime extension of energy storage in micro-grid applications," *IEEE Trans. Smart Grid*, vol. 4, no. 3, pp. 1289–1296, Jul. 2013.

[2] N. Mukherjee and D. Strickland, "Control of second-life hybrid battery energy storage system based on modular boost-multilevel buck converter," *IEEE Trans. Ind. Electron.*, vol. 62, no. 2, pp. 1034–1046, Jul. 2014.

[3] S. M. Goetz, Z. Li, X. Liang, C. Zhang, S. M. Lukic, and A. V. Peterchev, "Control of modular multilevel converter with parallel connectivity—Application to battery systems," *IEEE Trans. Power Electron.*, vol. 32, no. 11, pp. 8381–8392, Nov. 2017.

[4] M. Hagiwara and H. Akagi, "Experiment and simulation of a modular push–pull PWM converter for a battery energy storage system," *IEEE Trans. Ind. Appl.*, vol. 50, no. 2, pp. 1131–1140, Mar./Apr. 2014.

[5] I. Trintis, S. Munk-Nielsen, and R. Teodorescu, "A new modular multilevel converter with integrated energy storage," in *Proc. Annu. Conf. IEEE Ind. Electron. Soc.*, Nov. 2011, pp. 1075–1080.

[6] M. Vasiladiotis and A. Rufer, "Analysis and control of modular multilevel converters with integrated battery energy storage," *IEEE Trans. Power Electron.*, vol. 30, no. 1, pp. 163–175, Jan. 2015.

[7] M. Vasiladiotis, N. Cherix, and A. Rufer, "Impact of grid asymmetries on the operation and capacitive energy storage design of modular multilevel converters," *IEEE Trans. Ind. Electron.*, vol. 62, no. 11, pp. 6697–6707, May 2015.

[8] F. Gao, L. Zhang, Q. Zhou, M. Chen, T. Xu, and S. Hu, "State-of-charge balancing control strategy of battery energy storage system based on modular multilevel converter," in *Proc. IEEE Energy Convers. Congr. Expo.*, Sep. 2014, pp. 2567–2574.

[9] Q. Zhang, F. Gao, L. Zhang, and N. Li, "Multiple time scale optimal operation of MMC battery energy storage system," in *Proc. IEEE Energy Convers. Congr. Expo.*, Sep. 2015, pp. 1–7.

[10] N. Li, F. Gao, T. Hao, Z. Ma, and C. Zhang, "SOH balancing control method for the MMC battery energy storage system," *IEEE Trans. Ind. Electron.*, vol. 65, no. 8, pp. 6581–6591, Aug. 2018.

[11] Z. Ma, T. Hao, F. Gao, N. Li, and X. Gu, "Enhanced SOH balancing method of MMC battery energy storage system with cell equalization capability," in *Proc. IEEE Appl. Power Electron. Conf. Expo.*, 2018, pp. 3591–3597.

[12] N. Li, F. Gao, T. T. Yang, L. Zhang, Q. Zhang, and G. Q. Ding, "An integrated electric vehicle power conversion system using modular multilevel converter, "in *Proc. Energy Convers. Congr. Expo.*, Sep. 20–24, 2015, pp. 5044–5051.

[13] M. Quraan, T. Yeo, and P. Tricoli, "Design and control of modular multilevel converters for battery electric vehicles, "*IEEE Trans. Power Electron.*, vol. 31, no. 1, pp. 507–517, Jan. 2016.

[14] M. Quraan, P. Tricoli, S. D'Arco, and L. Piegari, "Efficiency assessment of modular multilevel converters for battery electric vehicles," *IEEE Trans. Power Electron.*, vol. 32, no. 3, pp. 2041–2051, Mar. 2017.

[15] D. Ronanki and S. S. Williamson, "Modular multilevel converters for transportation electrification: Challenges and opportunities," *IEEE Trans. Transp. Electrific.*, vol. 4, no. 2, pp. 399–407, Jun. 2018.

[16] L. Zhang, Yi Tang, S. Yang, and F. Gao, "A modular multilevel converter-based grid-tied battery-supercapacitor hybrid energy storage system with decoupled power control," in *Proc. IEEE Inter. Power Electron. Motion Control Conf.*, 2016, pp. 2964–2971.

[17] L. Zhang, Y. Tang, S. Yang, and F. Gao, "Decoupled power control for a modular multilevel converter-based hybrid AC-DC grid integrated with hybrid energy storage," *IEEE Trans. Ind. Electron.*, vol. 66, no. 4, pp. 2926–2934, Apr. 2019.

[18] T. Soong and P. W. Lehn, "Evaluation of emerging modular multilevel converters for BESS applications," *IEEE Trans. Power Del.*, vol. 29, no. 5, pp. 2086–2094, Oct. 2014.

[19] T. Soong and P. W. Lehn, "Internal power flow of a modular multilevel converter with distributed energy resources," *IEEE J. Emerg. Sel. Topic Circuits Syst.*, vol. 2, no. 4, pp. 1127–1138, Dec. 2014.

[20] Z. Ma, F. Gao, X. Gu, N. Li, and D. Niu, "An online SOH testing method of MMC battery energy storage system," in *Proc. IEEE 19th Workshop Control Model. Power Electron.*, 2018, pp. 1–7.

[21] P. Hu, D. Jiang, Y. Zhou, Y. Liang, J. Guo, and Z. Lin, "Energy-balancing control strategy for modular multilevel converters under submodule fault conditions," *IEEE Trans. Power Electron.*, vol. 29, no. 9, pp. 5021–5030, Sep. 2014.

[22] G. T. Son *et al.*, "Design and control of a modular multilevel HVDC converter with redundant power modules for noninterruptible energy transfer," *IEEE Trans. Power Del.*, vol. 27, no. 3, pp. 1611–1619, Jul. 2012.

[23] B. Li, Y. Zhang, R. Yang, R. Xu, D. Xu, and W. Wang, "Seamless transition control for modular multilevel converters when inserting a cold-reserve redundant submodule," *IEEE Trans. Power Electron.*, vol. 30, no. 8, pp. 4052–4057, Aug. 2015

[24] K. Li, L. Yuan, Z. Zhao, S. Lu, and Y. Zhang, "Fault-tolerant control of MMC with hot reserved submodules based on carrier phase shift modulation," *IEEE Trans. Power Electron.*, vol. 32, no. 9, pp. 6778–6791, Sep. 2017.

[25] F. Deng, Y. Tian, R. Zhu, and Z. Chen, "Fault-tolerant approach for modular multilevel converters under submodule faults," *IEEE Trans. Ind. Electron.*, vol. 63, no. 11, pp. 7253–7263, Nov. 2016.

[26] Q. Chen, R. Li, and X. Cai, "Analysis and fault control of hybrid modular multilevel converter with integrated battery energy storage system," *IEEE J. Emerg. Sel. Topics Power Electron.*, vol. 5, no. 1, pp. 64–78, Mar. 2017.

[27] J. Choi, B. Han, and H. Kim, "New scheme of phase-shifted carrier PWM for modular multilevel converter with redundancy submodules," *IEEE Trans. Power Del.*, vol. 31, no. 1, pp. 407–409, Feb. 2016.
[28] E. R. C. Da Silva, E. Cipriano Dos Santos, and C. B. Jacobina, "Pulsewidth modulation strategies," *IEEE Ind. Electron. Mag.*, vol. 5, no. 2, pp. 37–45, Jun. 2011.
[29] J. I. Leon, S. Kouro, L. G. Franquelo, J. Rodriguez, and B. Wu, "The essential role and the continuous evolution of modulation techniques for voltage-source inverters in the past, present, and future power electronics," *IEEE Trans. Ind. Electron.*, vol. 63, no. 5, pp. 2688–2701, May 2016.
[30] M. Hagiwara and H. Akagi, "Control and experiment of pulsewidth-modulated modular multilevel converters," *IEEE Trans. Power Electron.*, vol. 24, no. 7, pp. 1737–1746, Jul. 2009.
[31] M. Zhang, L. Huang, W. Yao, and Z. Lu, "Circulating harmonic current elimination of a CPS-PWM-based modular multilevel converter with a plug-in repetitive controller," *IEEE Trans. Power Electron.*, vol. 29, no. 4, pp. 2083–2097, Apr. 2014.
[32] K. Ilves, L. Harnefors, S. Norrga, and H. P. Nee, "Analysis and operation of modular multilevel converters with phase-shifted carrier PWM," *IEEE Trans. Power Electron.*, vol. 30, no. 1, pp. 268–283, Jan. 2015.
[33] D. G. Holmes and T. A. Lipo, *Pulse Width Modulation for Power Converters: Principles and Practice*. Hoboken, NJ, USA: Wiley, 2003.

Feng Gao (S'07–M'09–SM'18) received the B.Eng. and M.Eng. degrees in electrical engineering from Shandong University, Jinan, China, in 2002 and 2005, respectively, and the Ph.D. degree from the School of Electrical and Electronic Engineering, Nanyang Technological University, Singapore, in 2009.

From 2008 to 2009, he was a Research Fellow with Nanyang Technological University. Since 2010, he has been with the School of Electrical Engineering, Shandong University, where he is currently a Professor. From September 2006 to February 2007, he was a Visiting Scholar with the Department of Energy Technology, Aalborg University, Aalborg, Denmark.

Dr. Gao was the recipient of the IEEE Industry Applications Society Industrial Power Converter Committee Prize, for a paper published in 2006, and the IEEE Power Electronics Transactions Second Prize Paper Award in 2017. He is currently serving as the Associate Editor for the IEEE TRANSACTIONS ON POWER ELECTRONICS and CPSS TRANSACTIONS ON POWER ELECTRONICS AND APPLICATIONS.

Xin Gu received the B.Eng. and M.Eng. degrees in electrical engineering from Shandong University, Jinan, China, in 2015 and 2018, respectively.

In 2018, he joined Jinan Power Supply Company, State Grid Corporation of China, Jinan. His research interests include modular multilevel converters and battery energy storage system.

Zhan Ma (S'17) received the B.Eng. degree in electrical engineering from Shandong University, Jinan, China, in 2016. He is currently working toward the Ph.D. degree at the School of Electrical Engineering, Shandong University.

His research interests include battery management system, battery energy storage system, and modular multilevel converters.

Chenghui Zhang (M'14–SM'18) was born in China in 1963. He received the B.S. and M.S. degrees from Shandong University of Technology, Jinan, China, in 1985 and 1988, respectively, and the Ph.D. degree from Shandong University, in 2001.

In 1988, he joined Shandong University, where he is currently a Full Professor with the School of Control Science and Engineering and the Director of the Research Center of Power Electronics Energy-Saving Technology and Equipment of the Chinese Education Ministry. His research interests include optimal control of engineering, power electronics and motor drives, and energy-saving techniques.

Prof. Zhang was selected as a Changjiang Scholar of the Education Ministry and a Taishan Scholar of Shandong Province in 2009.